International Journal of Heat and Mass Transfer 112 (2017) 89–96

Contents lists available at ScienceDirect

International Journal of Heat and Mass Transfer

journal homepage: www.elsevier.com/locate/ijhmt

An experimentally validated method for temperature prediction during cyclic operation of a Li-ion cell

Divya Chalise [a], Krishna Shah [a], Tobias Halama [b], Lidiya Komsiyska [b], Ankur Jain [a,*]

[a] Mechanical and Aerospace Engineering Department, University of Texas at Arlington, Arlington, TX 76019, USA
[b] NEXT ENERGY · EWE Research Centre for Energy Technology e.V., 26129 Oldenburg, Germany

ARTICLE INFO

Article history:
Received 14 February 2017
Received in revised form 20 April 2017
Accepted 24 April 2017

Keywords:
Lithium ion battery
Thermal safety
Thermal modeling
Battery cooling

ABSTRACT

Li-ion batteries are used widely for electrochemical energy storage and conversion. Heat generation during the operation of a Li-ion cell results in large temperature rise, particularly at high discharge rates. Accurate prediction of temperature rise during operation is a key technical challenge that directly affects both performance and safety. Li-ion cells are often used in cyclic charge/discharge manner, making this a particularly important process to study. This paper presents an experimentally-validated analytical method to rapidly and accurately predict the temperature field in a Li-ion cell undergoing cyclic charge and discharge. Based on recursive solution of the governing energy equation during the cyclic process, this method computes temperature around 16X faster than finite-element simulations, and is found to be in very good agreement with experimental data for over fifty cycles of high-rate cycling of 18650 Li-ion cells. Results indicate that heat loss through the metal foil that provides electrical interconnection is a critical process that governs overall thermal behavior of the cell. A novel technique based on determining the effective heat transfer coefficient of the interconnection is described, which is shown to agree very well with experimental data. Results from this paper may be helpful for design of Li-ion cell systems, as well as real-time temperature prediction and performance optimization.

1. Introduction

Li-ion cells are used widely in energy conversion and storage devices due to excellent energy storage and power characteristics [1–3]. However, heat generation due to Ohmic and non-Ohmic mechanisms [4–7] during the operation of a Li-ion cell is a serious technological challenge [8,9]. It is well known that elevated temperatures dramatically reduce battery lifetime [9]. Even at temperature as low as 80 °C, degenerative processes begin to occur in a Li-ion cell, which cause severe safety issues and lead to thermal runaway [10]. Thus, the dissipation of generated heat through the cell material and into the ambient is an important transport process [8,9]. Impedance to thermal transport through various material interfaces in the cell [11,12] results in large temperature rise [13,14], which not only reduces electrochemical performance, but also leads to safety problems [15–17]. Such problems have been responsible for several recent, well-publicized events of thermal runaway and fire in batteries in automobiles, aircraft and consumer electronic devices.

It is critical to develop thermal management approaches for reducing temperature rise in a Li-ion cell [8,17]. This has been accomplished in the past through external mechanisms, such as the flow of a coolant over the outer surface of the cell [18], embedding the cell in a phase change material [19], the use of heat pipes [20], etc. Some limited work has also been carried out for internal cooling of a cell, for example by heat pipe insertion [21], by using current collector as a heat spreader [22] or by recirculating electrolyte [23] that acts as a coolant. In each case, it is important to accurately determine the cell temperature since it will govern whether thermal management is needed or not, and if so, the extent needed. Ideally, a temperature sensor must be present inside the cell to measure and report the cell temperature, which can be used for active control of thermal management. However, it is not always possible to embed temperature sensors within. Only a limited amount of work exists on internal temperature measurement of a Li-ion cell [24–29]. Due to these experimental limitations, the accurate prediction of temperature rise through mathematical modeling tools is critical. Such thermal prediction tools can play a key role in thermal management of cells, since accurate knowledge of the temperature rise in a cell can be used for proactive cooling of the cell. For example, a prediction of imminent temperature rise can be used for modulating the thermal

* Corresponding author.
E-mail address: jaina@uta.edu (A. Jain).

http://dx.doi.org/10.1016/j.ijheatmasstransfer.2017.04.115
0017-9310/

management system, or in an extreme case, completely shut down a cell to prevent thermal runaway. Temperature prediction is also critical for performance optimization, both at the design stage, as well as at run-time. For example, such tools can be used for evaluating and optimizing the thermal performance of a cell. During actual operation of a cell or a battery pack, accurate prediction of temperature rise can be a critical tool for performance optimization strategies such as load balancing.

Like in any other energy conversion system involving heat transfer, there are two distinct approaches for developing predictive tools for temperature rise in Li-ion cells. Finite-element simulation tools can be used for thermally modeling the operation of a Li-ion cell and numerically solving the governing energy equations along with appropriate boundary conditions to determine the temperature field in the Li-ion cell. A significant amount of literature already exists on such approaches [17]. On the other hand, an analytical approach can also be used where possible to derive an exact solution for the governing energy equation, resulting in an exact expression for the temperature rise. A limited amount of literature exists on the use of analytical methods for predicting temperature rise in Li-ion cells [13,14,30,31]. Both steady state and transient methods have been used on cylindrical as well as prismatic cells. Simulations are sometimes preferred due to the flexibility in geometry, thermal properties, etc. However, analytical methods have the advantage of being more accurate and faster to compute compared to numerical simulations. Further, in the context of Li-ion cells, analytical solutions may be preferable for implementation in battery management systems because these can be directly implemented and computed on a microprocessor instead of having to interface with a separate finite-element simulation code, which is often expensive, requires extensive computational power and is in general difficult to interface in real-time.

Cyclic charge and discharge of a Li-ion cell is of specific interest because it models the operation of the Li-ion cell in several realistic scenarios. Heat generation rate during a charge/discharge process is a key parameter that may govern temperature rise. Past measurements show that heat generation rate is a strong function of the discharge rate [7,12]. Key questions to address through the thermal modeling of a cyclic charge and discharge process include the effect of thermal properties and ambient thermal conditions on the temperature distribution in the cell, the effect of rest periods between successive discharges, and the role of electrical interconnection such as metal tabs on the cooling of the cell. The latter is a particularly important factor that has not been investigated much in the past. Since the metal tab or foil that electrically connects the cell to the power source and load usually has high thermal conductivity, its role in determining the temperature distribution of the cell is important to investigate.

This paper presents experimental measurement of temperature rise in a cylindrical 18650 cell during multiple successive cycles of charge and high-rate discharge, and a theoretical heat transfer model that accurately predicts the temperature rise under such conditions. The theoretical model accounts for thermal conduction within the cell, convection to the outside, as well as heat loss through the metal tabs connected to the cell poles. It is shown that heat loss through the metal tabs plays a critical role in determining the thermal behavior of the cell, and a novel technique to accurately account for this effect is discussed. These results demonstrate the capability of real-time computation of temperature distribution in the cell as a function of its electrochemical performance. This analytical approach is around 16X faster than finite-element simulations and offers the capability of close integration with electrical control components of a battery management system.

2. Experimental measurements

Commercially available high power Nickel Manganese Cobalt Oxide Li-ion cells of type INR18650-15L from Samsung are used for experimental measurements. The cells have a nominal capacity of 1500 mAh and internal resistance of 29.0 mΩ (±0.5 mΩ). Electrical connections are made via 0.3 mm thick Ni-coated steel foils welded to the poles. Prior to the measurements, the steel foil is soldered to a 1 mm thick copper plate. For the cycling tests, five cells are connected in parallel via screws to a 5 mm thick copper bar and placed in a temperature-controlled climate chamber (VC7034, Vötsch, Germany) maintained at 25 °C. Fig. 1(a) shows a picture of the prepared Li-ion cell. Fig. 1(b) shows a picture of the test environment. All cycling is conducted using a Maccor Series 4000 cell cycler. The five-cell string is charged initially with constant current of 7.5 A (1C) until voltage of 4.2 V is reached and then the voltage is kept constant until the current reaches 0.1 A. The constant voltage charging is followed by 10 min open circuit step. The discharge is performed with 52.5 A (7C) to a cut off voltage of 2.5 V with a subsequent open circuit step for 10 min. This sequence is repeated for 50 cycles. The temperature of each cell is monitored throughout the process using a Pt-100 temperature sensor attached to one of the cell poles. The sensor is configured in a four-wire circuit for improved measurement accuracy. The obtained temperature profiles as functions of time are used to validate the theoretical model.

3. Theoretical modeling

Consider a cylindrical, axisymmetric Li-ion cell of radius R, height H, mass density ρ and heat capacity C_p as shown in Fig. 1 (c). Assume the thermal conductivity of the cell to be orthotropic [32], with k_r and k_z as the radial and axial thermal conductivities respectively. The cell undergoes a cyclic charge/discharge process during which the temperature field within the cell as a function of time is of interest. In order to determine the temperature distribution, the cyclic process is split into N stages that occur in sequence. Each stage is characterized by a fixed heat generation rate Q_i, $i = 1, 2, \ldots N$. The duration of each stage is between $t_i = 0$ and $t_i = t_{F,i}$, where $t_{F,i}$ is the final time of the i^{th} stage. The cell is convectively cooled on the outside surfaces, which is modeled with convective heat transfer coefficients $h_{r,i}$ and $h_{z,i}$ applied on the curved surface, and top/bottom surfaces respectively. These coefficients may vary from one stage to another in order to model changes in convective cooling conditions between charge, discharge and rest stages.

The problem of determining the transient temperature distribution during the charge/discharge process may be solved in a recursive fashion by splitting the temperature distribution into temperature distributions during each stage, $T_i(r,z,t_i)$, so that the temperature field during the i^{th} stage is determined based on the temperature distribution at the end of the previous, $(i-1)^{\text{th}}$ stage.

Based on the problem description above, the transient temperature distribution in the Li-ion cell during the i^{th} stage is governed by the following energy conservation equation:

$$\frac{k_r}{r}\frac{\partial}{\partial r}\left(r\frac{\partial T_i}{\partial r}\right) + k_z\frac{\partial^2 T_i}{\partial z^2} + Q_i = \rho C_p\frac{\partial T_i}{\partial t_i} \tag{1}$$

Boundary conditions for this problem are as follows:

$$\frac{\partial T_i}{\partial r} = 0 \quad \text{at } r = 0 \tag{2}$$

$$k_r\left(\frac{\partial T_i}{\partial r}\right) = h_{r,i}\cdot T_i \quad \text{at } r = R \tag{3}$$

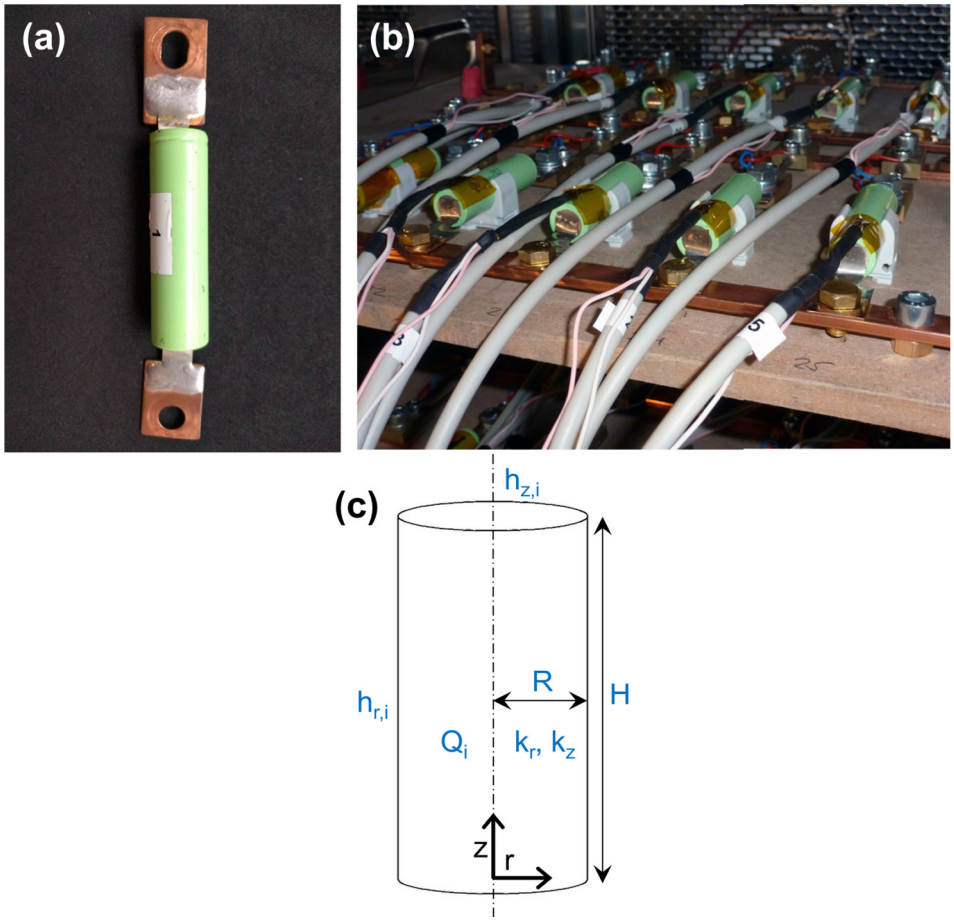

Fig. 1. (a) Picture of the 18650 Li-ion cell used for thermal measurements during high-rate, cyclic loading, (b) Picture of the experimental setup, (c) Schematic of the geometry of a single Li-ion cell undergoing cyclic charge and discharge.

$$k_z\left(\frac{\partial T_i}{\partial z}\right) = h_{z,i}\cdot T_i \quad \text{at z} = 0 \tag{4}$$

$$k_z\left(\frac{\partial T_i}{\partial z}\right) = -h_{z,i}\cdot T_i \quad \text{at z} = \text{H} \tag{5}$$

The recursion in solution of the temperature distribution occurs through the initial condition for this problem, which states that the initial temperature for the i^{th} stage is the same as the temperature at the end of the $(i-1)^{\text{th}}$ stage.

$$T_i(r,z,0) = T_{i-1}(r,z,t_{F,i-1}) \tag{6}$$

A solution for Eq. (1) subject to boundary conditions (2)–(5) and initial condition (6) can be derived using the method of separation of variables. To start with, the solution is written as

$$T_i(r,z,t_i) = u_i(r,z) + v_i(r,z,t_i) \tag{7}$$

where $u_i(r,z)$ and $v_i(r,z,t_i)$ provide the steady state and transient components of the solution respectively. $u_i(r,z)$ is determined first using the method of separation of variables, which provides the initial condition for determining $v_i(r,z,t_i)$. The final solution is found to be

$$u_i(r,z) = \frac{Q_i H^2}{4k_z}\left[\frac{z}{H} - \left(\frac{z}{H}\right)^2 + Bi_{H,i}^{-1}\right] + \sum_{n=1}^{\infty} A_{n,i} I_0(\lambda_{n,i} r)\left[\mu_{n,i}\cos(\mu_{n,i} z) + \frac{h_{z,i}}{k_z}\sin(\mu_{n,i} z)\right] \tag{8}$$

and

$$v_i(r,z,t_i) = \sum_{m=1}^{\infty}\sum_{n=1}^{\infty} A_{nm,i} J_0(\beta_{m,i} r)\left[\mu_{n,i}\cos(\mu_{n,i} z) + \frac{h_{z,i}}{k_z}\sin(\mu_{n,i} z)\right] \exp\left(-\alpha(\lambda_{n,i}^2 + \beta_{m,i}^2)\cdot t_i\right) \tag{9}$$

The eigenvalues $\mu_{n,i}H$ and $\beta_{m,i}R$ are roots of the following equations respectively

$$\tan(\mu_{n,i}H) = \frac{2(\mu_{n,i}H)Bi_{H,i}}{(\mu_{n,i}H)^2 - Bi_{H,i}^2} \tag{10}$$

and

$$Bi_{R,i} J_0(\beta_{m,i}R) - (\beta_{m,i}R) J_1(\beta_{m,i}R) = 0 \tag{11}$$

where $\lambda_{n,i} = \sqrt{\frac{k_r}{k_z}}\mu_{n,i}$, $Bi_{H,i} = \frac{h_{z,i}H}{k_z}$ and $Bi_{R,i} = \frac{h_{r,i}R}{k_r}$.

Further, note that the coefficients in equations (8) and (9) are given by

$$A_{n,i} = \frac{\int_0^H -h_{r,i}\frac{Q_i H^2}{4k_z}\left[\frac{z}{H} - \left(\frac{z}{H}\right)^2 + Bi_{H,i}^{-1}\right]\left[\mu_{n,i}\cos(\mu_{n,i} z) + \frac{h_{z,i}}{k_z}\sin(\mu_{n,i} z)\right]dz}{\frac{1}{2}\left[\left(\mu_{n,i}^2 + \left(\frac{h_{z,i}}{k_z}\right)^2\right)H + 2\frac{h_{z,i}}{k_z}\right](k_r\lambda_{n,i} I_0'(\lambda_{n,i}R) + h_{r,i} I_0(\lambda_{n,i}R))} \tag{12}$$

and

$$A_{nm,i} = \frac{\int_0^H\int_0^R r[T_{0,i}(r,z) - u_i(r,z)]J_0(\beta_{m,i} r)\left[\mu_{n,i}\cos(\mu_{n,i} z) + \frac{h_{z,i}}{k_z}\sin(\mu_{n,i} z)\right]drdz}{\frac{1}{4\beta_{m,i}^2}\left[\left(\mu_{n,i}^2 + \left(\frac{h_{z,i}}{k_z}\right)^2\right)H + 2\frac{h_{z,i}}{k_z}\right][Bi_{R,i}^2 + (\beta_{m,i}R)^2][J_0(\beta_{m,i}R)]^2} \tag{13}$$

where $T_{0,i}$ is the initial temperature for the i^{th} stage.

Eqs. (7) through (13) complete the definition of the solution, which provides the temperature distribution in the i^{th} stage based on $T_{0,i}$, the initial temperature of the i^{th} stage, which is the same as the final temperature of the previous stage. For the very first stage, the initial condition is obtained from the initial condition of the overall problem, which is used to solve the temperature distribution for $i = 1$, the first stage. This solution is then used to obtain the initial condition for $i = 2$, the second stage, and the procedure is repeated recursively until the temperature distribution in each stage has been determined.

4. Results and discussion

Fig. 2 presents a comparison of experimental measurement of the cell temperature, measured at the end-face of the cell with predictions from the analytical model presented in Section 3 for over fifty consecutive cycles. Fig. 2 also shows the measured variation in current as a function of time during this process. Fig. 2 shows excellent agreement between experimental data and the analytical thermal model over a very long time period. The degree of agreement can be seen better in Figs. 3 and 4 that show this comparison for only the first five and last five cycles respectively. The maximum deviation between the two is less than 1.0 °C, or around 5.7% over all fifty cycles. The highest deviation typically occurs around the end of the discharge, when temperature is the highest. During the remaining of the operation, the experimental data and analytical model are in even better agreement. Key contributors towards the small deviation most likely include the assumption of constant heat generation during charge or discharge and the values of convective heat transfer coefficients for the analytical model. Moreover, given that the deviation is mostly less than 1 K for most of the duration of the experiment, uncertainties in the experimental setup and measurement accuracy could also contribute to the small deviation. Regardless, the good agreement observed over a large number of cycles is encouraging and demonstrates the capability of the model to accurately predict thermal behavior of a Li-ion cell during operation.

Note that in order to compute the thermal model, thermal properties of the 18650 cell including k_r, k_z, C_p and ρ are taken from past measurements [32]. Heat generation rates during charge and discharge are determined from previous measurements based on the C-rates implemented in the experiment [7]. Since these data were obtained for a 26650 cell, a volumetric scaling is carried out to estimate heat generation rate of the 18650 cell. A convective heat transfer coefficient of h = 10 W/m^{2}K corresponding to natural convection is assumed on the radial outer surface of the cell. At the end-surface, a higher value of h = 205 W/m^{2}K is used during the low-current charge and open circuit rest periods in order to account for enhanced heat loss during these periods through the metal foil that provides electrical connection to the end-face of the cell. This value is estimated from a separate finite-element simulation of the electrical connection to the cell, discussed later in this section. The modeled time durations for each charge, discharge and rest period are based on the experimental cell cycling data.

Heat loss from the outer surfaces of the cell plays a key role in determining the thermal response of the cell. While heat transfer from the radial outer surface of the cell may reasonably be expected to occur through natural convection when the cell is not being actively cooled, as is the case in these experiments, heat transfer from the end surfaces of the cell may be more complicated due to the presence of metal foil tabs that electrically connect the cell to the power source or load. Such metal tabs typically have high thermal conductivity and may therefore conduct significant

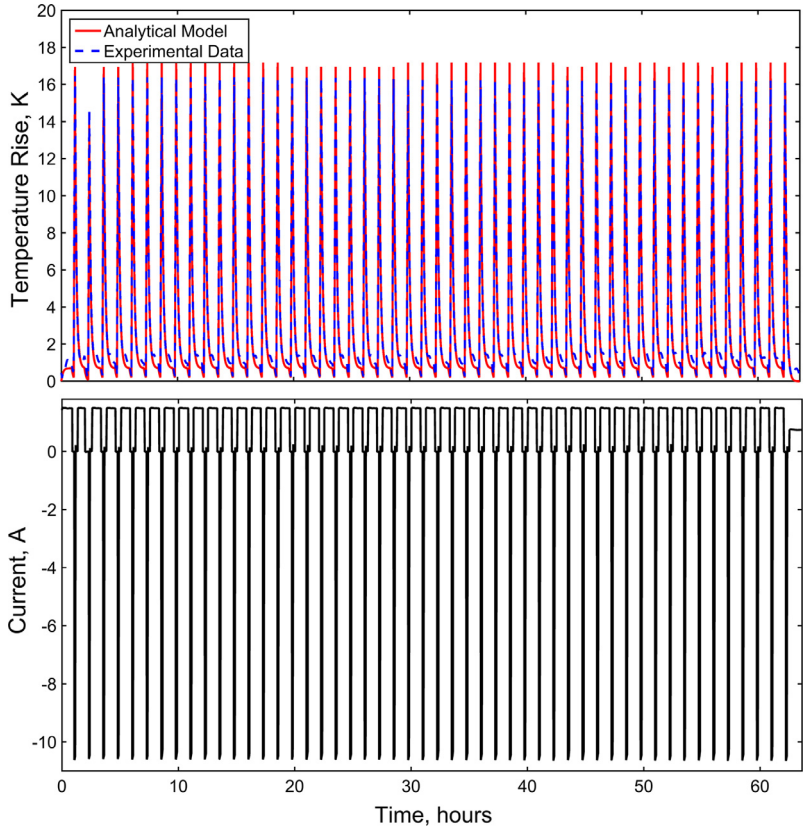

Fig. 2. Comparison of experimental measurement and analytical computation of the end-surface temperature of a 18650 cell undergoing over fifty charge-discharge-rest cycles. Very good agreement is found over all fifty cycles.

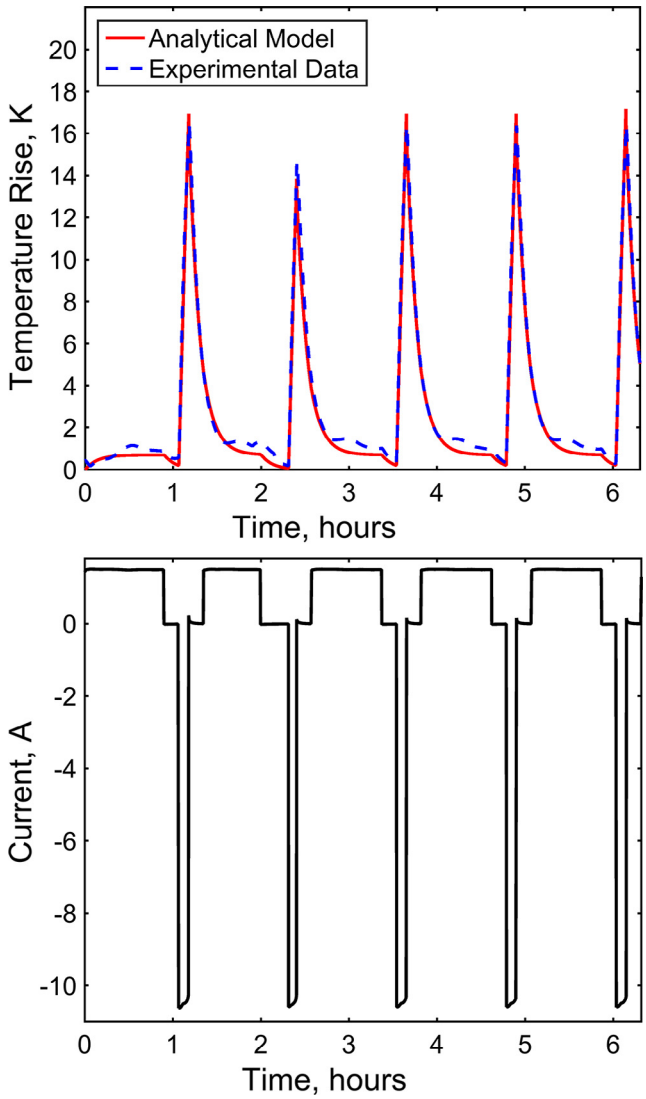

Fig. 3. Comparison of experimental measurement and analytical computation of the end-surface temperature of an 18650 cell during the first five cycles of a multi-cycle process.

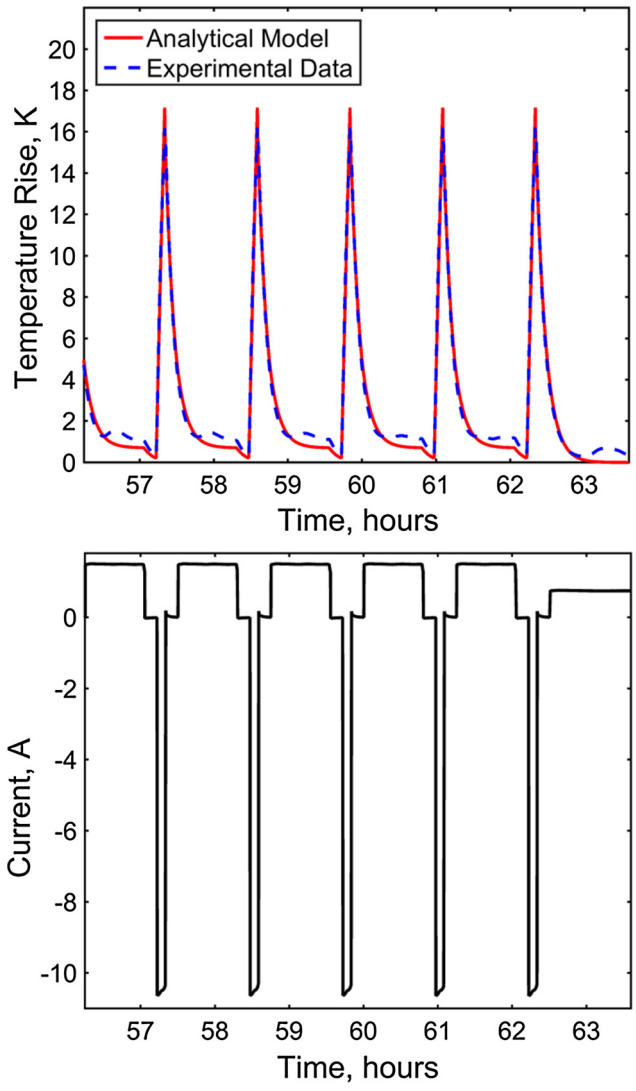

Fig. 4. Comparison of experimental measurement and analytical computation of the end-surface temperature of an 18650 cell during the last five cycles of a multi-cycle process.

amount of heat. In addition, during high-rate discharge, the metal foil may also be generating heat due to Joule heating from the high current, and therefore may only have a limited heat removal role during high rate discharge. It is important to account for the role of the metal foil in determining the thermal response of the cell. In this case, this is done by carrying out a separate finite-element thermal simulation to determine the total thermal resistance of the metal foil assembly, and calculating the effective heat transfer coefficient representative of this total thermal resistance, which is then used in the analytical model during the charge and cooloff periods. The geometry of the metal foil is shown in Fig. 5(a). A constant temperature boundary condition is applied on the cell face in a finite-element simulation, which is used to determine the total heat loss from the cell face through the metal foil into the ambient, assumed to be at zero temperature. The temperature distribution from the simulation is shown in Fig. 5(b).The total thermal resistance of the metal foil is then calculated as the ratio of the applied temperature difference to the total heat flow. The effective heat transfer coefficient, determined from the definition of Newton's law of cooling is found to be 205 W/m^2K, which is significantly larger than the typical value of 10 W/m^2K for natural convection conditions. This shows that there is significant heat loss through the metal tab during charge and cooloff periods when the foil does not generate any heat by itself and therefore acts as a thermal fin to remove additional heat from the cell. On the other hand, during high-rate discharge, the fin effect is eliminated because the foil itself generates Joule heating. Fig. 6 presents a comparison of experimental data with the theoretical model computed without and with consideration of the fin effect of the metal foil. When the fin effect is neglected, heat loss from the ends occurs only through natural convection, with a low value of h. On the other hand, when the fin effect is taken into account, the value of h is larger, as computed from the finite-element simulations described above. Fig. 6 clearly shows much better agreement with experimental data when the fin effect is accounted for. The predicted temperature is too large without the fin effect, and is much closer to experimental data with the fin effect. This demonstrates the importance of heat loss through the metal foil that provides electrical interconnection to the cell. Even though heat removal is not the key function of the metal foil, it is nevertheless an important phenomenon primarily due to the high thermal conductivity of the foil. Determining and implementing an effective heat transfer coefficient as outlined above results in improved accuracy of

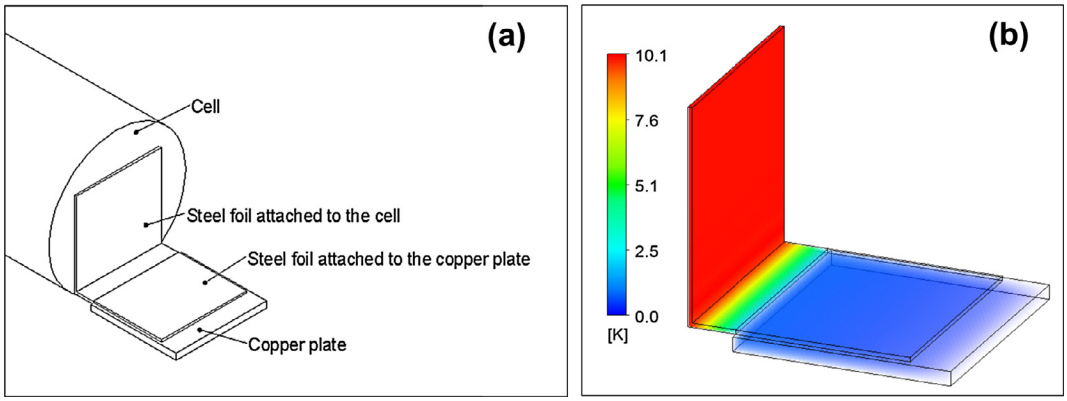

Fig. 5. (a) Schematic geometry of the metal foil attached to the end-face of a Li-ion cell for electrical interconnection, (b) Temperature distribution in the metal foil due to an imposed temperature gradient, for determination of the effective heat transfer coefficient of the metal foil.

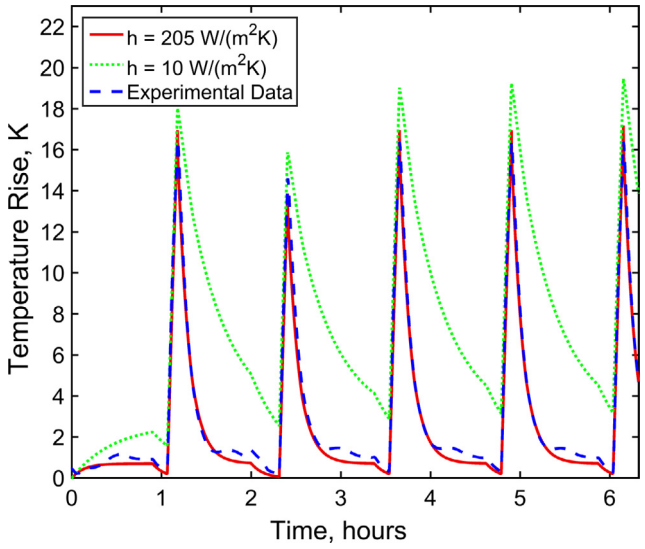

Fig. 6. Comparison of experimental data for temperature rise during five cycles and analytical model without and with consideration of heat loss through the metal foil. This comparison shows that heat loss through the metal foil is important and must be accounted for.

the temperature prediction. This is also an effective approach since it combines the effects of geometry, configuration, etc. into a single effective heat transfer coefficient. Based on specific geometry, thermal properties and other parameters associated with a given problem, the effective heat transfer coefficient needs to be calculated only once through analysis of a simple finite-element simulation as outlined here.

For further validation of the analytical model, a comparison is carried out against finite-element simulations in ANSYS CFX 15.0. The same geometry, boundary and heat generation rates are specified in the simulations as in the analytical model. The grid for finite-element simulations is chosen to be fine enough so that there is no grid-dependence of the results. The grid chosen for the final simulation utilizes 1.26 million elements. Fig. 7 compares temperature as a function of time predicted by the analytical model with finite-element simulations for 50 consecutive cycles. A zoomed-in plot for first five cycles only is shown in Fig. 8. There is very good agreement between the two over all 50 cycles, with a peak deviation of less than 1.8 °C, or 10.8% that occurs at the end of the discharge cycle. For most of the remainder of the period, the agreement is even better. Note that the peak temperature reached at the end of each discharge varies from cycle to cycle due to differences in the discharge times, which are obtained from experimental data. The good agreement with finite-element simulations provides further validation of the analytical model. In comparison with finite element simulation models, the analytical model computes temperatures much faster. For example, for the first five cycles, the finite-element simulation takes around 4839 s, excluding the time for geometry setup and grid generation, whereas the analytical model takes 290 s to compute the entire

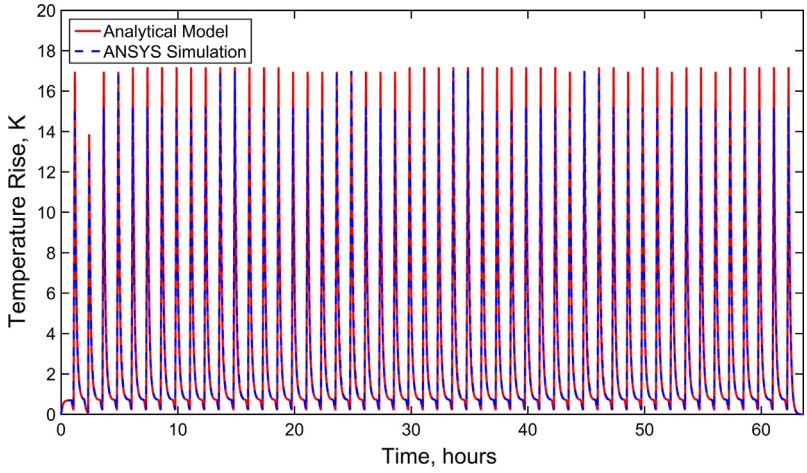

Fig. 7. Comparison of the analytical model with finite-element simulations results for a large number of cycles.

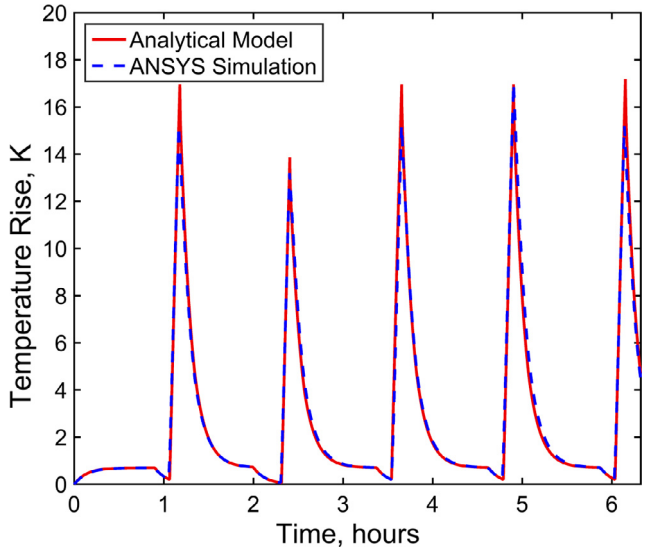

Fig. 8. Comparison of the analytical model with finite-element simulations results for the first five cycles only.

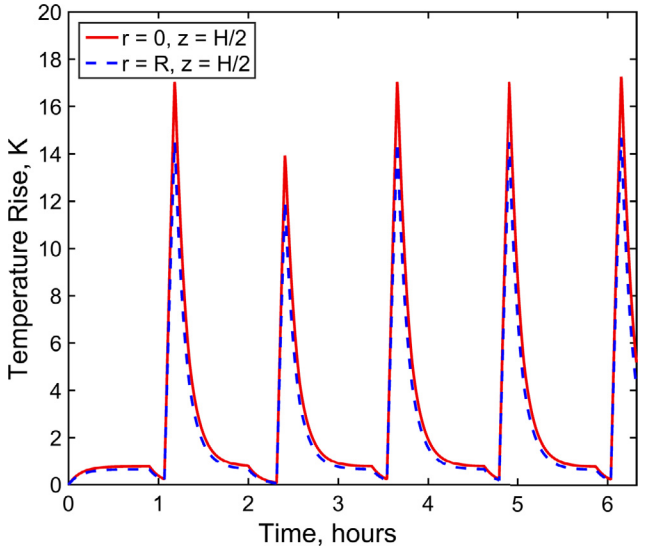

Fig. 10. Core and outside surface temperatures of a 18650 Li-ion cell undergoing cyclic loading, as predicted by the experimentally-validated analytical model. Results demonstrate the capability to predict core temperature that may be useful for design and real-time performance optimization.

temperature field with ten eigenvalues, and only 15 s for a single eigenvalue.

The analytical treatment in Section 2 derives the temperature distribution in the form of an infinite series. In practice, only a finite number of terms can be computed to determine the temperature. The number of eigenvalues to be used is important, because in general, increasing the number of eigenvalues is expected to improve accuracy at the expense of increased computation time. Fig. 9 plots temperature as a function of time determined from the analytical model for five charge-rest-discharge-rest cycles, computed with 1, 5 and 10 eigenvalues. This plot shows very little difference between these three cases, indicating that even a single eigenvalue results in reasonably accurate computation of the temperature field. There is only a minor discontinuity in the predicted temperature with a single eigenvalue, which is fixed by the use of five eigenvalues. As a result, it may be reasonable to consider only the first five terms in the summations in eqs. (8) and (9) without much loss of accuracy. Computation of temperature with a single eigenvalue reduces the computation time by 20X compared to ten eigenvalues. This is a useful insight for implementation of this model for real-time temperature prediction in battery management systems.

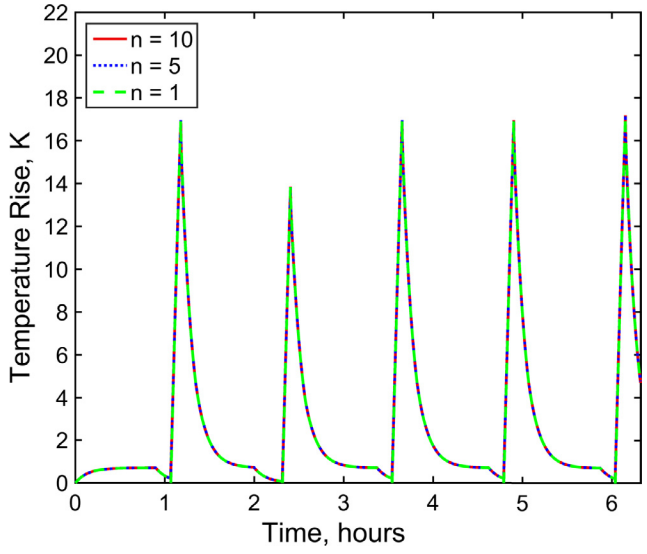

Fig. 9. Effect of the number of eigenvalues on temperature predicted by the analytical model over five cycles. Results indicate that even a single eigenvalue provides reasonable accuracy.

The experimentally validated model is capable of a wide variety of temperature computations for cyclic operation of a Li-ion cell. For example, Fig. 10 plots the core temperature and the outside surface temperature of a Li-ion cell undergoing a multi-cycle process similar to the experiments described in Section 2. As expected, the core temperature is larger than the outside temperature, particularly at the end of each discharge, when it is as much as 15% greater. The capability to accurately predict the core temperature, enabled by this analytical model is critical, because most experimental techniques are unable to directly measure the core temperature without invasive insertion of a temperature sensor into the Li-ion cell. The analytical model in this paper, validated through experimental measurements provides a useful tool for analyzing what-if scenarios as well as real-time monitoring of the core temperature of the cell. Such information can be valuable for thermal design of the cell and the cyclic charge/discharge process, as well as for run-time performance management such as load redistribution based on core temperature.

5. Conclusions

A Li-ion cell is commonly subjected to cyclic charge and discharge for energy conversion and storage. Temperature rise during such processes is important since excessive heating may lead to performance reduction and safety issues such as thermal runaway. This paper presents experimental validation of a recursive thermal model that accurately predicts the temperature rise during a cyclic process by splitting the process into a number of stages, and deriving a solution for the temperature profile during each stage based on the temperature distribution at the end of the previous stage. Experimental data on cylindrical NMC 18650 cells undergoing high rate discharge over a large number of cycles are in very good agreement with the model predictions. This work demonstrates the importance of accounting for heat loss through the metal tabs that provide electrical interconnection, and shows that determining the

effective convective heat transfer coefficient of the current conductor tab may be an effective means of doing so. The method described here computes temperature around 16X faster than finite-element simulations and is much easier to integrate with battery management systems. Results from this paper may be helpful for effective design, as well as run-time thermal and multi-disciplinary performance optimization.

Acknowledgments

This material is based upon work supported by CAREER Award No. CBET-1554183 from the National Science Foundation. The authors would like to thank Daniel Trapp from NEXT ENERGY for technical support regarding experimental cell cycling.

References

[1] B. Scrosati, J. Hassoun, Y.-K. Sun, Lithium-ion batteries. A look into the future, Energy Environ. Sci. 4 (9) (2011) 3287–3295, http://dx.doi.org/10.1039/C1EE01388B.
[2] R.A. Marsh, S. Vukson, S. Surampudi, B.V. Ratnakumar, M.C. Smart, M. Manzo, P. J. Dalton, Li ion batteries for aerospace applications, J. Power Sources 97 (2001) 25–27, http://dx.doi.org/10.1016/S0378-7753(01)00584-5.
[3] A. Khaligh, Z. Li, Battery, ultracapacitor, fuel cell, and hybrid energy storage systems for electric, hybrid electric, fuel cell, and plug-in hybrid electric vehicles: State of the art, IEEE Trans. Vehic. Technol. 59 (6) (2010) 2806–2814, http://dx.doi.org/10.1109/TVT.2010.2047877.
[4] V. Srinivasan, C.Y. Wang, Analysis of electrochemical and thermal behavior of Li-ion cells, J. Electrochem. Soc. 150 (1) (2003) A98–A106, http://dx.doi.org/10.1149/1.1526512.
[5] K.E. Thomas, J. Newman, Heats of mixing and of entropy in porous insertion electrodes, J. Power Sources 119 (2003) 844–849, http://dx.doi.org/10.1016/S0378-7753(03)00283-0.
[6] D. Bernardi, E. Pawlikowski, J. Newman, A general energy balance for battery systems, J. Electrochem. Soc. 132 (1) (1985) 5–12, http://dx.doi.org/10.1149/1.2113792.
[7] S. Drake, M. Martin, D.A. Wetz, J.K. Ostanek, S.P. Miller, J.M. Heinzel, A. Jain, Heat generation rate measurement in a Li-ion cell at large C-rates through temperature and heat flux measurements, J. Power Sources 285 (2015) 266–273, http://dx.doi.org/10.1016/j.jpowsour.2015.03.008.
[8] K. Shah, V. Vishwakarma, A. Jain, Measurement of multiscale thermal transport phenomena in Li-ion cells: a review, ASME J. Electrochem. Energy Convers. Storage 13 (030801) (2016) 1–13, http://dx.doi.org/10.1115/1.4034413.
[9] T.M. Bandhauer, S. Garimella, T. Fuller, A critical review of thermal issues in Lithium-ion batteries, J. Electrochem. Soc. 158 (3) (2011) R1–R25, http://dx.doi.org/10.1149/1.3515880.
[10] R. Spotnitz, J. Franklin, Abuse behavior of high-power Lithium-ion cells, J. Power Sources 113 (1) (2003) 81–100, http://dx.doi.org/10.1016/S0378-7753(02)00488-3.
[11] V. Vishwakarma, C. Waghela, Z. Wei, R. Prasher, S.C. Nagpure, J. Li, F. Liu, C. Daniel, A. Jain, Heat transfer enhancement in a Lithium-ion cell through improved material-level thermal transport, J. Power Sources 300 (2015) 123–131, http://dx.doi.org/10.1016/j.jpowsour.2015.09.028.
[12] Y. Ye, L.H. Saw, Y. Shi, K. Somasundaram, A.A.O. Tay, Effect of thermal contact resistances on fast charging of large format lithium ion batteries, Electrochim. Acta 134 (2014) 327–337, http://dx.doi.org/10.1016/j.electacta.2014.04.134.
[13] K. Shah, S.J. Drake, D.A. Wetz, J.K. Ostanek, S.P. Miller, J.M. Heinzel, A. Jain, An experimentally validated transient thermal model for cylindrical Li-ion cells, J. Power Sources 271 (2014) 262–268, http://dx.doi.org/10.1016/j.jpowsour.2014.07.118.
[14] K. Shah, S.J. Drake, D.A. Wetz, J.K. Ostanek, S.P. Miller, J.M. Heinzel, A. Jain, Modeling of steady-state convective cooling of cylindrical Li-ion cells, J. Power Sources 258 (2014) 374–381, http://dx.doi.org/10.1016/j.jpowsour.2014.01.115.
[15] Q. Wang, P. Ping, X. Zhao, G. Chu, J. Sun, C. Chen, Thermal runaway caused fire and explosion of lithium ion battery, J. Power Sources 208 (2012) 210–224, http://dx.doi.org/10.1016/j.jpowsour.2012.02.038.
[16] K. Shah, D. Chalise, A. Jain, Experimental and theoretical analysis of a method to predict thermal runaway in Li-ion cells, J. Power Sources 330 (2016) 167–174, http://dx.doi.org/10.1016/j.jpowsour.2016.08.133.
[17] R. Zhao, S. Zhang, J. Liu, J. Gu, A review of thermal performance improving methods of lithium ion battery: electrode modification and thermal management system, J. Power Sources 299 (2015) 557–577, http://dx.doi.org/10.1016/j.jpowsour.2015.09.001.
[18] N. Nieto, L. Diaz, J. Gastelurrutia, F. Blanco, J.C. Ramos, A. Rivas, Novel thermal management system design methodology for power lithium-ion battery, J. Power Sources 272 (2014) 291–302, http://dx.doi.org/10.1016/j.jpowsour.2014.07.169.
[19] C.V. Hémery, F. Pra, J.F. Robin, P. Marty, Experimental performances of a battery thermal management system using a phase change material, J. Power Sources 270 (2014) 349–358, http://dx.doi.org/10.1016/j.jpowsour.2014.07.147.
[20] Z. Rao, S. Wang, M. Wu, Z. Lin, F. Li, Experimental investigation on thermal management of electric vehicle battery with heat pipe, Energy Convers. Manag. 65 (2013) 92–97, http://dx.doi.org/10.1016/j.enconman.2012.08.014.
[21] D. Anthony, D. Wong, D. Wetz, A. Jain, Improved thermal performance of a Li-ion cell through heat pipe insertion, J. Electrochem. Soc. (2016), in review.
[22] S. Pannala, H. Wang, K. Kepler, S. Allu, Thermal management for high-capacity large format Li-Ion cells, Electrochem. Soc. (2014) 445, MA2014-02.
[23] S.K. Mohammadian, Y.L. He, Y. Zhang, Internal cooling of a lithium-ion battery using electrolyte as coolant through microchannels embedded inside the electrodes, J. Power Sources 293 (2015) 458–466, http://dx.doi.org/10.1016/j.jpowsour.2015.05.055.
[24] D. Anthony, D. Sarkar, A. Jain, Non-invasive, transient determination of the core temperature of a heat-generating solid body, Sci. Rep. 6 (35886) (2016) 1–10, http://dx.doi.org/10.1038/srep35886.
[25] R. Srinivasan, B.G. Carkhuff, M.H. Butler, A.C. Baisden, O.M. Uy, An external sensor for instantaneous measurement of the internal temperature in lithium-ion rechargeable cells, Proc. SPIE 8035, Energy Harvest. and Storage: Mater., Devices, and Appl. II (2011), http://dx.doi.org/10.1117/12.884691, 80350D.
[26] G. Zhang, L. Cao, S. Ge, C.Y. Wang, C.E. Shaffer, C.D. Rahn, In situ measurement of radial temperature distributions in cylindrical li-ion cells, J. Electrochem. Soc. 161 (10) (2014) A1499–A1507, http://dx.doi.org/10.1149/2.0051410jes.
[27] M.S.K. Mutyala, J. Zhao, J. Li, H. Pan, C. Yuan, X. Li, In-situ temperature measurement in lithium ion battery by transferable flexible thin film thermocouples, J. Power Sources 260 (2014) 43–49, http://dx.doi.org/10.1016/j.jpowsour.2014.03.004.
[28] S. Novais, M. Nascimento, L. Grande, M.F. Domingues, P. Antunes, N. Alberto, C. Leitão, R. Oliveira, S. Koch, G.T. Kim, S. Passerini, Internal and external temperature monitoring of a Li-ion battery with Fiber Bragg grating sensors, Sensors 16 (2016) 1394, http://dx.doi.org/10.3390/s16091394.
[29] C. Forgez, D.V. Do, G. Friedrich, M. Morcrette, C. Delacourt, Thermal modeling of a cylindrical LiFePO4/graphite lithium-ion battery, J. Power Sources 195 (2010) 2961–2968, http://dx.doi.org/10.1016/j.jpowsour.2009.10.105.
[30] K. Shah, A. Jain, Modeling of steady-state and transient thermal performance of a Li-ion cell with an axial fluidic channel for cooling, Int. J. Energy Res. 39 (2015) 573–584.
[31] P. Taheri, M. Yazdanpour, M. Bahrami, Analytical assessment of the thermal behavior of nickel metal hydride batteries during fast charging, J. Power Sources 245 (2014) 712–720, http://dx.doi.org/10.1016/j.jpowsour.2013.06.086.
[32] S.J. Drake, D.A. Wetz, J.K. Ostanek, S.P. Miller, J.M. Heinzel, A. Jain, Measurement of anisotropic thermophysical properties of cylindrical Li-ion cells, J. Power Sources 252 (2014) 298–304, http://dx.doi.org/10.1016/j.jpowsour.2013.11.107.